基于摆动旋转电弧的焊枪空间姿态识别

李湘文， 洪 波， 尹 力， 洪宇翔
（湘潭大学 机械工程学院，湘潭 411105）

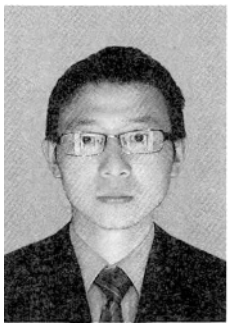

李湘文

摘 要：通过对现有电弧传感器的扫描信号进行深入研究，提出了一种摆动旋转电弧传感器，在分析其信号特点的基础上，推导出焊枪空间姿态与弧长变化之间的数学关系，建立了该电弧传感器的弧长数学模型. 考虑到焊接电弧信号的特点与复杂性，采用了 Gabor 小波滤波器来消除信号中的噪声干扰，并对滤波后的采样数据进行了特征向量提取，降低了数据的维度，根据欧式距离的原理设计了焊枪姿态分类器，采用模型参数的最速下降法对焊枪的空间姿态进行了实时识别. 结果表明，摆动旋转电弧传感器的焊枪空间姿态识别算法简单、获取信息量大，为提高焊缝跟踪的精度提供了理论依据.

关键词：焊缝跟踪；摆动旋转电弧；焊枪姿态识别；Gabor 小波
中图分类号：TP242.2 **文献标识码**：A **文章编号**：0253－360X(2013)04－0035－03

0 序 言

焊接是一个复杂的热加工过程，焊件受热变形，造成坡口和焊道位置发生变化，需要对焊枪的位置和姿态进行实时修正[1,2]. 另外，由于目前电弧传感器扫描信号比较单一，容易造成采样数据样本重叠现象，很难精确提取出焊枪的空间位置信息.

为了有效地解决电弧传感器的焊缝跟踪问题，进一步提高焊缝跟踪精度，针对不同电弧传感器的电弧传感信号进行深入分析，提出摆动旋转电弧传感器并建立摆动旋转弧长数学模型，推导出焊枪空间姿态与弧长变化之间的数学关系，研究了基于摆动旋转电弧的焊枪空间姿态识别方法，最后通过对不同焊枪空间姿态识别进行了试验验证，证明这种方法的有效性和正确性.

1 摆动旋转电弧传感器信号分析

目前，识别焊枪姿态的电弧传感器主要有摆动式和旋转式[3]，摆动式电弧传感器又可分为直线摆动和曲线摆动两种，由于传感器电弧扫描轨迹的不同，电弧传感信号中包含的焊缝位置、焊枪姿态等信息差别很大，下面简要介绍这几种传感器的电弧传感信号特征.

直线摆动电弧传感器如图 1a 所示，焊枪在水平放置的工件上左右直线扫描摆动，电弧信号只包含 x 轴线上的焊缝信息，因此，从电弧传感信号中只可提取到焊枪在 x 轴上的偏移量. 曲线摆动电弧传感器如图 1b 所示，焊枪做曲线锥摆，电弧运动可以等效看作其在 xOy 平面上对图 1b 所示的阴影部分区域扫描，因此从电弧信号中可以提取到 xOy 平面内的信息. 旋转电弧传感器如图 1c 所示，焊枪在 xOz 平面上扫描图 1c 所示的阴影部分区域，从而可以提取到焊枪在 xOz 平面内的信息.

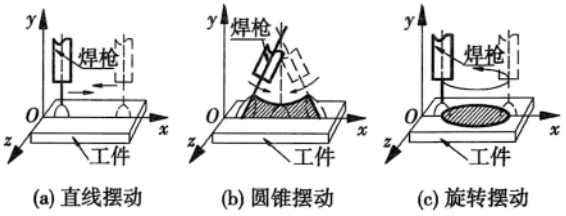

图 1 电弧传感器的摆动模型

Fig. 1 Arc sensor model

由于实际焊枪的姿态是三维空间的，而上述的电弧传感器很难提取空间姿态信息，文中提出摆动旋转电弧传感器方案，是在旋转电弧传感器的基础上结合圆锥摆动，同时具有摆动和旋转的特点，且摆动和旋转的信号特征相互正交、互不干扰，因此，摆动旋转电弧传感器的电弧扫描运动属于空间扫描，

收稿日期：2012－04－15
基金项目：国家自然科学基金资助项目(50975243)；湖南省教育厅重点资助项目(11A114)；湖南省研究生科研创新资助项目(CX2012B257)

可提取的姿态信息量增多.

2 焊枪空间姿态识别系统

针对目前还没有很好的算法适用于空间焊缝姿态的提取,文中在视觉姿态识别算法的基础上提出了基于统计学习的姿态识别方法. 该识别系统的结构框图如图 2 所示.

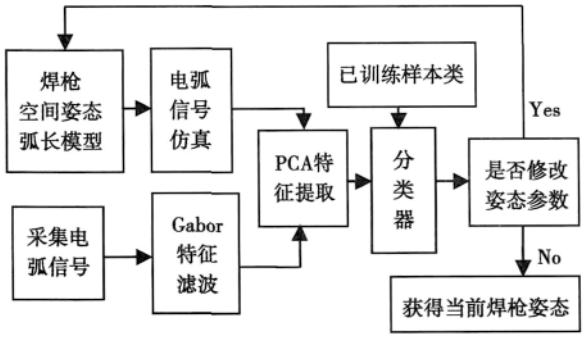

图 2 焊枪空间姿态识别系统结构框图

Fig. 2 Structure diagram of recognition system of welding torch gesture

2.1 焊枪姿态弧长模型

建立摆动旋转电弧传感器的弧长模型之前,先假设旋转电弧传感器的旋转频率 f 是摆动频率的 $4N$ 倍($N \in 1,2\cdots$),N 取值越大,精度越高,但实时性变差,数据量也越大,一般取 $N=2$. 当摆动器以 δ 为摆动角做圆锥摆动,同时旋转电弧传感器以 r 为旋转半径旋转,则摆动旋转电弧传感器的导电嘴端部的运动方程可表示为

$$\left.\begin{aligned} x_t &= r\cos\delta_t \sin 2\pi f\cdot t + L\sin\delta_t \\ y_t &= L(1-\cos\delta_t) + r\sin\delta_t \sin 2\pi f\cdot t \\ z_t &= r\cos 2\pi f\cdot t \\ \delta_t &= \arcsin\left(\tan\delta\cdot\sin\frac{\pi f t}{2N}\right) \end{aligned}\right\} \quad (1)$$

式中: x_t, y_t, z_t 为摆动旋转电弧传感器在任意时刻的空间位置; L 为摆动器的顶点到焊枪导电嘴的距离; δ_t 为摆动器任意时刻摆动的角度.

以 V 形坡口焊缝为例,设坡口开角为 α,当焊枪姿态处于焊缝正中心处时,弧长模型可表示为

$$h(t) = \frac{x_t(L+H_c)}{(x_t\cot\alpha + L - y_t)\sin\delta_t} \quad (2)$$

式中: H_c 为焊枪导电嘴端部到工件的距离.

但在实际焊接中,焊枪不一定时刻居中,焊枪的空间位置除了在 x,y,z 轴上的偏移,还包括轴上的偏移角,一般定义载体的 x,y,z 三个方向构成右手系,绕 z 轴旋转就是横滚角,绕 x 轴旋转就是俯仰角,绕 y 轴旋转就是航向角. 这样可以设焊枪在 xOz 平面上投影与 z 轴的夹角称为航向角,用 β 表示; 焊枪在 xOy 平面上投影与 y 轴的夹角称横滚角,用 θ 表示; 焊枪在 yOz 平面上投影与 y 轴的夹角称为俯仰角,用 γ 表示.

则焊枪导电嘴端部的空间姿态矩阵可表示为

$$\boldsymbol{A} = \mathrm{trans}(vx,\Delta D_e)\ \mathrm{rot}(x,\gamma)\ \mathrm{trans}(y,\Delta H_e)\ \mathrm{rot}(y,\beta)\ \mathrm{trans}(z,\Delta W_e)\ \mathrm{rot}(z,\theta) \quad (3)$$

式中: ΔD_e 为电弧中心与焊缝中心的 x 方向偏移量; ΔH_e 为焊炬高度的 y 方向偏移量; ΔW_e 为电弧中心与焊缝中心的 z 方向偏移量.

焊枪导电嘴端部的空间姿态有

$$(x,y,z,1)^{\mathrm{T}} = \boldsymbol{A}(x_t,y_t,z_t,1)^{\mathrm{T}} \quad (4)$$

根据式(1) ~式(4),任意时刻,对于三维空间姿态的焊枪,弧长高度的变化可表示为

$$h(t) = \frac{|\boldsymbol{A}_1|(L+H_c)}{(|\boldsymbol{A}_1|\cot\alpha + |\boldsymbol{A}|L - |\boldsymbol{A}_2|)\sin\delta_t} \quad (5)$$

式中: A_1, A_2 用如下公式表示

$$\boldsymbol{A}_1 = \begin{bmatrix} x & -c\beta s\theta & s\beta & \Delta W_e\cdot s\beta + \Delta D_e \\ y & -s\gamma s\beta s\theta + c\gamma c\theta & -s\gamma c\beta & -\Delta W_e\cdot s\gamma c\varphi + \Delta H_e\cdot c\gamma \\ z & c\gamma s\beta s\theta + s\gamma c\theta & c\gamma c\beta & \Delta W_e\cdot c\gamma c\varphi + \Delta H_e\cdot s\gamma \\ 1 & 0 & 0 & 1 \end{bmatrix}$$

$$\boldsymbol{A}_2 = \begin{bmatrix} c\beta c\theta & x & s\beta & \Delta W_e\cdot s\beta + \Delta D_e \\ s\gamma s\beta c\theta + c\gamma s\theta & y & -s\gamma c\beta & -\Delta W_e\cdot s\gamma c\varphi + \Delta H_e\cdot c\gamma \\ -c\gamma s\beta c\theta + s\gamma s\theta & z & c\gamma c\beta & \Delta W_e\cdot c\gamma c\varphi + \Delta H_e\cdot s\gamma \\ 0 & 1 & 0 & 1 \end{bmatrix}$$

式中: $c\beta, s\beta, c\theta, s\theta, c\gamma, s\gamma$ 分别表示为 $\cos\beta, \sin\beta, \cos\theta, \sin\theta, \cos\gamma, \sin\gamma$.

根据理论研究和试验结果可知[4],当电弧动态变化时,弧长变化的幅值与电流变化的幅值成正比关系,则通过式(5)便可获得焊枪任意空间姿态的变化与焊接电流间的关系.

2.2 电弧传感信号的 Gabor 滤波

焊接时,电弧的电流信号、电压信号是由长时低频成分和短时高频成分组成的非平稳信号,对于非平稳的奇异信号在信号的突变处包含有丰富的信息量,所以希望有一种滤波器在低频部分有高的频率分辨率、低的时间分辨率,在高频部分有低的频率分辨率、高的时间分辨率[5]. Gabor 小波核函数能够捕捉对应于空间频率(尺度)、空间位置以及方向选择性的局部结构信息,正好满足以上特性. 文中采用 Gabor 滤波器来消除由于焊接中短路过渡以及电弧

飞溅造成的白噪声等影响,不仅降低了数据维度,而且可以获得精度比较高的数据信息.

2.3　PCA 特征提取

虽然采样后 Gabor 特征矢量的维数已经明显降低,但仍然是高维特征,一种处理高维特征问题的方法是通过提取特征来降低维数,其中基于主成分(PCA)特征特别引人注目[6].

假设 Gabor 滤波后的数据有 N 个样本,用 t 维的特征矢量 $x_i(i=1,2,\cdots,N)$ 表示,PCA 可以找到一个线性变换矩阵将 t 维的原始特征矢量映射到 n 维的子空间,其中 $n \ll t$. 在进行 PCA 变换之前,首先对每个样本数据 x_i 进行数据标准化,转换为符合正态分布的矢量 x'_i,然后再组合构成矩阵 $X=[x'_1,x'_2,\cdots,x'_N]$,则其协方差矩阵 $Q=X\cdot X^{\mathrm{T}}$,求协方差矩阵的特征值和特征向量为

$$\lambda E = QE \tag{6}$$

式中: E 为单位特征向量; λ 为特征值,将特征值按照大小排序,取前 n 列本征矢量即得到 $t\times n$ 的线性变换矩阵 W_{pca}. 新的特征向量可以表示为

$$y_i = W_{\mathrm{pca}}^{\mathrm{T}} x_i \quad (i=1,2,\cdots,N) \tag{7}$$

式中: x_i 为 t 维的列向量; $W_{\mathrm{pca}}^{\mathrm{T}}$ 为 W_{pca} 的转置; y_i 为 n 维的列向量. 可以看出 PCA 能够大幅降低原始特征维数,而且保留了重要数据的特征量.

2.4　分类器的设计

焊枪姿态识别是一个多类识别任务,文中采用欧式距离分类器,对未知姿态的焊接电流数据的特征空间与已训练数据样本对应的特征向量之间的欧式距离进行计算,未知姿态的焊接电流数据与哪种模型数据的距离最近,就将其归入该类.

假设已训练的焊枪姿态分有 m 类,分别为 w_1, $w_2,\cdots,w_{\mathrm{m}}$,每类都有一个对应的特征空间向量,则共有 m 个特征空间向量,分别记作 $T_1,T_2,\cdots,T_{\mathrm{m}}$. 则未知焊枪姿态的特征向量 x 与 w_i 类的已训练焊枪姿态特征向量 T_i 之间的欧氏距离为

$$\begin{aligned} d_i(x) &= d(x_i,T_i) = \| x_i - T_i \| \\ &= \sqrt{(x_i-T_i)^{\mathrm{T}}(x_i-T_i)} \quad (i=1,2,\cdots,N) \end{aligned} \tag{8}$$

未知焊枪姿态的特征向量 x 与 m 类已训练的焊枪姿特征空间向量分别求欧式距离后,得到一个距离集 d_1, $d_2,\cdots,d_{\mathrm{m}}$,如果对所有的 $i\neq j$,都有 $d_i(x) < d_j(x)$. 即 $d_i(x)$ 是距离集中最小的值,则将当前焊枪姿态的特征向量 x 归入第 w_i 类.

2.5　基于模型参数的姿态计算

获得当前焊枪姿态的特征类后,还需要计算当前焊枪姿态的准确数值,文中采用模型参数的最速下降法来进行姿态参数识别,具体步骤如下所述.

焊枪姿态参数识别,目的是求解模型参数的最优化问题,目标函数为多维变量,其中: $\bar{x}^{(0)}=(\bar{x}_1^{(0)},\bar{x}_2^{(0)},\cdots,\bar{x}_n^{(0)})^{\mathrm{T}}$, $\bar{x}_{\mathrm{n}}^{(0)}$ 取焊枪模型的空间姿态参量 β、γ、θ、ΔDe、ΔWe、ΔHe; 首先固定前 $n-1$ 个自变量 $\bar{x}_1^{(0)},\bar{x}_2^{(0)},\cdots,\bar{x}_{\mathrm{n}-1}^{(0)}$,使用二次多项式近似法及外推内插法搜索自变量 $\bar{x}_{\mathrm{n}}^{(0)}$ 直到满足

$$\| \nabla f(\bar{x}^{(k+1)}) \| - \| \nabla f(\bar{x}^{(k)}) \| \leqslant \varepsilon \tag{9}$$

式中: ε 为迭代计算精度.

然后替代 $\bar{x}^{(0)}=\bar{x}^{(k)}$,再固定 $n-1$ 个变量 $\bar{x}_1^{(0)}$, $\bar{x}_2^{(0)},\cdots,\bar{x}_{n-2}^{(0)},\bar{x}_{\mathrm{n}}^{(0)}$,用二次多项式逼近法和外推内插法搜索,直到再次满足式(9). 这样一步步迭代求出 n 个变量的最优值,从而获得当前焊枪姿态的准确数值.

3　焊枪姿态识别试验分析

为了检验研究方法在焊枪姿态识别的效果,作者进行了大量焊接试验,具体试验条件如下: 焊接电源为松下 KR350,焊接方法为 CO_2 气体保护焊,母材为 Q235-A,焊接电流 260 A、电压 29 V、气体流速 20 L/min、焊炬高度 $H_{\mathrm{e}}=15$ mm、旋转频率 24 Hz、旋转半径 1 mm、摆动频率 3 Hz、摆幅角 5°. 已训练原始数据样本按类别分别选择编号为 RF,RB,RU,RD,LF,LB,LU,LD,ZF,ZB,Z(对应右前、右后、右上、右下、左前、左后、左上、左下、正前、正后、正面等 11 种姿态)的焊接电弧数据各一组进行训练,共产生 11 组特征空间. 试验中首先判定当前采样数据样本的焊枪姿态属于 11 类特征空间的哪一类,再根据这一类包含的姿态数去修改模型参数,从而识别出当前焊枪姿态.

表 1 为焊枪姿态识别结果. 从表 1 的试验结果可以看出,通过分类器识别姿态类别的识别结果都在 92% 以上,平均识别率更是达到了 95.8%,识别准确率较高,更进一步说明通过 Gabor + PCA 的识别方案除了明显降低了特征维数之外,还增加了焊枪姿态的区分度,使其更易于分类识别.

表 1　焊枪姿态识别结果

Table 1　Result of welding-torch gesture recognition

特征姿态类别	识别率(%)		识别时间
	分类器	姿态	t/ms
$\beta,\Delta D_{\mathrm{e}}$	98.4	96.5	12
$\beta,\theta,\Delta W_{\mathrm{e}},\Delta H_{\mathrm{e}}$	96.6	77.6	35
$\beta,\gamma,\theta,\Delta De,\Delta We,\Delta He$	92.3	65.1	69
平均	95.8	82.5	38.7

[下转第 52 页]

849.

[3] Tao K, Zhou X L, Cui H, *et al*. Oxidation and hot corrosion behaviors of HVAF-sprayed conventional and nanostructured NiCrC coatings [J]. Transactions of Nonferrous Metals Society of China, 2007, 19(5): 1151 - 1160.

[4] Subhash K, Jayaganthan R, Satya P. Evaluation of cyclic hot corrosion behavior of detonation gun sprayed Cr_3C_2-25% NiCr coatings on nickel-and iron-based superalloys [J]. Surface & Coatings Technology, 2009, 203(8): 1004 - 1013.

[5] Gurrappa I. Hot Corrosion Behavior of CM 247 LC alloy in Na_2SO_4 and NaCl environment [J]. Oxidation of Metals, 1991, 51(2): 353 - 382.

[6] Yuuzou K. High temperature corrosion mechanisms and effect of alloying elements for materials used in waste incineration environment [J]. Corrosion Science, 2002, 44(2): 223 - 245.

[7] Sobolev V V, Guilemany J M. Investigation of coating porosity formation during High-Velocity Oxy-Fuel (HVOF) spraying [J], Materials Letters, 1994, 18(5/6): 304 - 308.

[8] Calvarin G, Molins R, Huntz A M. Oxidationmechanism of Ni-20Cr foils and its relation to the oxide-scale microstructure [J]. Oxidation of Metals, 2000, 53(1/2): 25 - 48.

[9] Otero E, Pardo A, Perosanz F J, *et al*. Surface modification of several steels after their exposure at high temperature to oxygen and sulfur mixtures [J]. Surface & Coatings Technology, 1995, 76(1/3): 53 - 60.

[10] Bala N, Singh H, Prakash S. Accelerated hot corrosion studies of cold spray Ni-50Cr coating on boiler steels [J]. Materials and Design, 2010, 31(1): 244 - 253.

[11] 王从曾. 材料性能学 [M]. 北京: 北京工业大学出版社, 2001.

[12] Krishnaveni K, Narayanan T S N S, Seshadri S K. Electroless Ni-B coatings: preparation and evaluation of hardness and wear resistance [J]. Surface & Coating Technology. 2005, 190(1): 115 - 121.

[13] 何肇基. 金属的力学性质 [M]. 北京: 冶金工业出版社, 1989.

作者简介: 赵晓舟,男,1986 年出生,硕士研究生. 主要从材料表面工程技术研究. Email: 603011866@qq.com

通讯作者: 周 正,男,博士. Email: zhouzhengbjut@bjut.edu.cn

[上接第 37 页]

但随着需要识别姿态的特征维数增加,最速下降法识别焊枪姿态的识别率逐渐降低. 实验表明对于焊枪姿态的识别,可通过减少特征维度来提高识别率,但此时的姿态识别效果会受到一定程度的影响,实际应用中要根据试验情况对比删除不需要识别的特征维数,以提高识别率,加速识别响应.

4 结 论

(1) 提出了一种新型的电弧传感器—摆动旋转电弧传感器,建立摆动旋转弧长数学模型并推导出焊枪空间姿态与弧长变化之间的数学关系.

(2) 采用 Gabor 滤波器不仅消除了焊接中由于短路过渡以及电弧飞溅造成的噪声干扰,而且对特征提取时间减少,特征维数降低, 计算量和内存需求减少.

(3) 在焊枪姿态识别中,PCA 的降维处理,可以大幅降低特征维数, 从而使计算量大幅降低. 试验结果表明 PCA 的特征值提取,对提高焊枪的姿态识别率具有重要意义.

(4) 通过求解欧氏距离和焊枪姿态模型参数的识别计算而获得当前焊枪姿态的类别以及各姿态量,实验表明需要识别的焊枪位姿量越少,识别的效率越高,识别的响应越快.

参考文献:

[1] 李志刚, 张 华, 高延峰. 旋转电弧传感器特征谐波法的改进 [J]. 焊接学报, 2009, 30(5): 54 - 56.
Li Zhigang, Zhang Hua, Gao Yanfeng. Improvement of characteristic harmonic method in rotational arc sensor [J]. Transactions of the China Welding Institution, 2009, 30(5): 54 - 56.

[2] Murayama V L, Rao V S. Mathematical modeling of simple seam tracking process applicable in multi - function control robotic welding system [J]. Journal of the Institution of Engineers (India), 2004, 85(9): 20 - 26.

[3] 叶建雄. 旋转电弧传感焊枪倾角检测及水下焊缝跟踪技术研究 [D]. 南昌: 南昌大学, 2007.

[4] 潘际銮. 现代 弧焊控制 [M]. 北京: 机械工业出版社, 2000.

[5] 冯曰海, 刘 嘉, 殷树言, 等. 新型低飞溅高能量短路过渡波形控制技术 [J]. 焊接学报, 2009, 27(8): 45 - 48.
Feng Yuehai, Liu Jia, Yan Shuyan, *et al*. The new type of low spatter and high energy waveform control technology for short-circuiting welding [J]. Transactions of the China Welding Institution, 2009, 27(8): 45 - 48.

[6] 杜健辉, 石永华, 王国荣, 等. 基于 PCA Nu-SVR 的水下焊缝偏差识别方法 [J]. 焊接学报, 2011, 27(3): 21 - 24.
Du Jianhui, Shi Yonghua, Wang Guorong, *et al*. Seam offset identification of underwater arc welding using PCA Nu-SVR [J]. Transactions of the China Welding Institution, 2011, 27(3): 21 - 24.

作者简介: 李湘文,男,1982 年出生,博士,讲师. 主要从事焊接设备及自动化等方面的科研和教学工作. 发表论文 3 篇. Email: hongbo@xtu.edu.cn.

welding; pulsed laser beam welding; tensile property; cupping property

Effects of keyhole-assisted gas jet on microstructure and microhardness of stainless steel laser weld SHEN Xianfeng, HUANG Wenrong, TENG Wenhua, XU Chao (Institute of Machinery Manufacturing Technology, China Academy of Engineering Physics, Mianyang 621900, China). pp 19 – 22

Abstract: Slab CO_2 continuous wave laser welding of HR-2 hydrogen-resistance stainless steel was carried out with different keyhole-assisted gas jet. During welding, the incident angle of the keyhole-assisted gas jet was 60° with a nozzle put ahead of the laser beam. The experimental results show that the layout with gas nozzle ahead of laser beam obtained better weld appearance and had little perturbation on the welding pool than that with gas nozzle behind the laser beam in gas jet-assisted keyhole laser welding. Compared with traditional laser welding, penetration depth increased significantly while penetration width decreased, and the weld shape became gourd-like with narrow middle part and wide upper and lower parts in the enhanced laser welding, because more plasma was suppressed within the keyhole and the keyhole deepened. Shorter columnar grains formed near the fusion line while equiaxed grain existed in the center of weld in enhanced laser welding, and the weld solidified by following ferrite-austenite (FA) mode. The reason for less ferrite precipitated in the weld could be resulted from the introduction of keyhole-assisted gas jet which improved the cooling condition of the weld metal.

Key words: gas jet-assisted keyhole laser welding; assisted gas jet; penetration increase; hydrogen-resistance stainless steel; microstructure

Effect of arc-ultrasonic excitation current on pores and tensile properties of MGH956 alloy TIG weld LEI Yucheng[1,2], HUANG Wei[1], XIA Xiaoping[3], ZHAO Kai[1], XIAO Bo[1] (1. School of Materials Science and Engineering, Jiangsu University, Zhenjiang 212013, China; 2. Jiangsu Province Key Laboratory of High-End Structural Materials, Jiangsu University, Zhenjiang 212013, China; 3. Tianjin Xingang Shipbuilding Heavy Industry Co., Ltd, Tianjin 300456, China). pp 23 – 26

Abstract: The arc-ultrasonic can be excited by modulating the TIG arc through high frequency. The mechanism of arc-ultrasonic was analyzed, and the effect of excitation current on pores and tensile strength of the MGH956 alloy joint made with TIG welding process was investigated. Without arc-ultrasonic, when the excitation current was 5 A and 10 A, pores in the weld obviously grew up, although the amount of pores kept almost the same. When the excitation current increased to 20 A and 30 A, the amount of pores decreased. With arc-ultrasonic, the tensile strength of the resultant joint was improved and reached the optimum value 550 MPa, 76% of that of base metal, when the excitation current was 20 A. The joints fractured with mixed brittle-ductile features.

Key words: MGH956 alloy; arc-ultrasonic; tungsten inert gas welding; pore

Mechanical properties of iron-based hard coatings prepared by plasma spraying technology LEI Ali, FENG Lajun, SHEN Wenning, WANG Guanchong (School of Materials Science and Engineering, Xi'an University of Technology, Xi'an 710048, China). pp 27 – 30

Abstract: In order to prepare wear-resistant coating on the surface of carbon steels and make the expansion coefficient of coating close to that of substrate and reduce stress in coating, mechanically mixed powders of 80% Fe, 13% P and 7% C were used to prepare iron-based wear-resistant coating by plasma spraying. The bonding strength was tested using binder dual tensile test method. The hardness in the coating was analyzed by surface microhardness method. And the wear resistance test of coating was carried out by MMW-2 (high temperature) friction and wear testing machine using 40Cr cemented carbide as grinding materials. The results show that the average bonding strength of the coating was 29 MPa, and the average microhardness was 805 HV50, higher than that of ceramic coating. The coating had better wear resistance, and the coating abrasion loss was around 36 mg which was about 1/13 of the grinding material. And the wear mechanism of the coating was mainly abrasive wear.

Key words: thermal spray; hard coating; bonding strength; microhardness; wear resistance

Effect of material flow on flash formation during continuous driven friction welding JI Shude[1], LIU Jianguang[2], ZHANG Liguo[1], ZOU Aili[1], FU Li[1] (1. Faculty of Aerospace Engineering, Shenyang Aerospace University, Shenyang 110136, China; 2. National Key Laboratory for Precision Hot Processing of Metals, Harbin Institute of Technology, Harbin 150001, China). pp 31 – 34

Abstract: The 2D coupled thermo-mechanical model was established to numerically simulate the effects of temperature and material flow on the flash formation of ring parts during continuous driven friction welding. The calculated results show that the material in friction stage mainly flew axially, while the radial velocity was nearly zero. During the forging stage, the material in or near the edge of friction surface mainly flew along the radial direction under large axial forging pressure, which resulted in the formation of flash. And the dimensions and bending degree of the flash increased with increasing of welding time, rotating speed and axial forging pressure. Based on the shape of flashes, suitable welding parameters were determined for continuous driven friction welding of 45 steel ring structures.

Key words: continuous driven friction welding; material flow; flash; numerical simulation

Recognition of spatial attitude of welding torch based on swing of rotating arc LI Xiangwen, HONG Bo, YIN Li, HONG Yuxiang (College of Mechanical Engineering, Xiangtan University, Xiangtan 411105, China). pp 35 – 37, 52

Abstract: Based on researches on scanning signal of existing arc sensors, a kind of oscillating rotating arc sensor was put forward. After analyzing the signal characteristics of the new arc sensor, the mathematical relationship between spatial attitude

of welding torch and the change of arc length was deduced, and a mathematical model was established for the arc length. Considering the characteristics and complexity of welding arc signal, the Gabor wavelet filter was used to eliminate the noise interference, and the feature vector was extracted from the sample data after filtering, and the dimension of data was reduced. The classifier of welding torch attitude according to the principle of Euclidean distance, real-time identification of the spatial attitude of welding torch was conducted with the steepest descent method of model parameters. The results show that the algorithm for recognition of spatial attitude of welding torch with swing of rotating arc sensor was simple and provided theoretical basis for improving the precision of welding seam tracking.

Key words: spatial attitude; welding torch; rotating arc; arc sensor; welding seam tracking

Low temperature sintering-bonding through in-situ formation of Ag nanoparticles using micro-scaled Ag_2O composite paste MU Fengwen[1], ZOU Guisheng[1], ZHAO Zhenyu[1], WU Aiping[1], YAN Jiuchun[2], Y. Norman Zhou[1,3] (1. Key Laboratory for Advanced Materials Processing Technology (Ministry of Education), Department of Mechanical Engineering, Tsinghua University, Beijing 100084, China; 2. State Key Laboratory of Advanced Welding & Joining, Harbin Institute of Technology, Harbin 150001, China; 3. Department of Mechanical and Mechatronics Engineering, University of Waterloo, Waterloo N2L 3G1, Canada). pp 38 - 42

Abstract: In order to reduce the cost of using Ag nanoparticle paste as bonding materials in electronic packaging, micro-scaled Ag_2O powders were mixed with triethylene glycol (TEG) to form a paste to replace the Ag particle paste. The reaction mechanism of in-situ formation of Ag nanoparticles, the sintering characteristics of micro-Ag_2O paste at low temperature, and the bonding of Ag-coated Cu bulks using this paste were investigated. The results reveal that the Ag_2O particles in the paste were more easily transformed into Ag nanoparticles than micro-Ag_2O itself, and with increasing the sintering temperature, more Ag nanoparticles formed and grew larger by sintering, accompanied with some gaseous products which could escape easily. The effect of sintering-bonding time on the strength of joints fabricated at 250 ℃ under a pressure of 2 MPa was analyzed. The average shear strength of the joints increased with sintering-bonding time and reached about 24 MPa when the sintering-bonding time was 5 min. And the microstructure of the fractured surface and the cross-section of typical joints made at 250 ℃ under 2 MPa were also examined.

Key words: silver oxide; in-situ formation; Ag nanoparticles; sintering bonding

Diagnosis of welding arc ionization region and boundary XIAO Tianjiao, SONG Yonglun, LI Chao, YAN Sibo (School of Mechanical Engineering and Applied Electronics Technology, Beijing University of Technology, Beijing 100123, China). pp 43 - 47

Abstract: Welding arc, as a heat source, converts electric energy to heat energy by gas discharging, and the scale of the arc ionization region as well as the effective range of the arc determines the distribution of its energy density. In this paper, the quantitative detection of argon atoms and argon-ion line intensity were achieved by emission spectroscopy diagnostic method, and the arc ionization region and the gas atom excitation radiation boundary scale were obtained. The measurement not only overcame the problem that the arc could not be quantitatively tested with camera due to exposure factors, but also could be used for observation of pulsed arc. The results provide the basis for better understanding arc physics and modeling the arc.

Key words: tungsten inert gas welding; arc boundary; ionization region; arc geometric pattern; spectroscopy diagnostic

Corrosion and wear behavior of wire-arc sprayed Ni-based coatings ZHAO Xiaozhou[1], ZHOU Zheng[1], HE Dingyong[1], ZHAO Qiuying[2], LI Ran[1], JIANG Jianmin[1] (1. College of Materials Science and Engineering, Beijing University of Technology, Beijing 100124, China; 2. Postdoctoral Research Station of Mechanical Engineering, Beijing University of Technology, Beijing 100124, China). pp 48 - 52

Abstract: A new Ni-based cored wire was designed to prepare coatings by wire-arc spraying on SA 213-T2 substrate in order to solve the corrosion and wear problems in waste-to-energy (WTE) plants. According to X-ray diffractometry (XRD) and scanning electron microscopy (SEM) analysis, the as-deposited coatings with low content of oxide phases presented uniform and dense layered structure with porosity at around 3%. The wear resistance of the designed coating, about 7 times higher than that of the substrate, was measured by a rubber wheel abrisive testing machine. Thermo-gravimetric technique was used to investigate the high-temperature corrosion behavior of the coatings in molten salt environment (Na_2SO_4 - 10% NaCl) at 800 ℃ in a muffle furnace. As a result, the weight gain curve of the coating followed the parabolic law and presented extremely lower corrosion rates, comparing with that of the substrate, due to the formation of Cr_2O_3 and $NiCr_2O_4$ oxide films on the surface which prevented the diffusion or penetrating of corrosive species. Consequently, the developed coating could provide much better corrosion resistance properties than SA213-T2 substrate.

Key words: Ni-based coating; arc spraying; microstructure; hot corrosion; wear behavior

Recognition of weld flaw based on feature fusion of ultrasonic signal and image HU Wengang, GANG Tie (State Key Laboratory of Advanced Welding and Joining, Harbin Institute of Technology, Harbin 150001, China). pp 53 - 56

Abstract: Ultrasonic testing is widely applied to detect the inner flaws of materials, but it is still difficult to recognize the flaw properties. In this paper, a new method for flaw recognition based on feature fusion of ultrasonic signal and image was proposed. The detection data was used to identify the weld flaw by the data fusion of ultrasonic signal feature and morphological feature. The welds containing defects such as hole, slag, crack,